31st Congress of the International Council of the Aeronautical Sciences

Belo Horizonte, Brazil; September 09-14, 2018

APPLICABILITY OF GEOMETRICALLY-LINEAR STRUCTURAL-DYNAMIC MODELS FOR THE FLIGHT DYNAMICS OF ARBITRARILY-FLEXIBLE AIRCRAFT

Antônio B. Guimarães Neto* , **Flávio L. Cardoso-Ribeiro*** , **Flávio J. Silvestre***
***Instituto Tecnológico de Aeronáutica, São José dos Campos, SP, 12228-900, Brazil**

Keywords: *aeroelasticity, flight dynamics, flexible aircraft, small deformations, large deformations*

Abstract

The assumption of small deformations in the formulation of the flight dynamics of flexible aircraft can be very convenient as it allows the use of a reduced number of modes of vibration to represent the structural dynamics with little loss of accuracy. However, depending on the level of structural flexibility, deformations may become large enough to violate this simplifying assumption, making geometrically-nonlinear formulations necessary. Delimiting the range of validity of small deformations is then indispensable for the flight-mechanics engineer in state-of-the-art aircraft design. In this paper, small- and large-deformation formulations are compared in equilibrium conditions and in time-marching simulations for aircraft with different levels of structural flexibility. The importance of geometrical nonlinearities and the range of validity of small deformations are assessed.

1 Introduction

A methodology to assess the validity of the assumption of small deformations in geometrically-linear structural-dynamic models was proposed and applied to an idealized aircraft model by Guimarães Neto et al. [1]. The methodology is simple and self-contained because it depends only on the geometrically-linear model itself, not requiring the availability of geometrically-nonlinear models to compare with.

The methodology is based on the fact that the linear rigid-body modes of the structural-dynamic model are representative if, and only if, small deformations occur. Hence, considering the formulation proposed by Guimarães Neto et al. [1], if two different support locations are considered, one at a time, one near the center of mass and the other in the region of maximum deformations with respect to a mean-axis system (in aircraft structures, typically the wing tips), the conversion of the elastic displacement vector from one condition to the other using linear rigid-body modes is possible with minimum error if, and only if, small deformations occur.

In Ref. [1], this methodology was applied without comparison of the geometrically-linear with a -nonlinear formulation. The first part of the additional work of comparison between dissimilar formulations was done by Guimarães Neto et al. [2], including equilibrium conditions and small disturbances around such conditions.

Formulations based on the simplifying assumption of small deformations have long been available and used in flight dynamics of flexible aircraft. Quasi-static analysis techniques as proposed by Rodden and Love [3] and implemented in MSC Nastran [4] are among the main uses of geometrically-linear aeroelastic finite-element method (FEM) models.

The simplifying assumption can also be considered in dynamically-coupled formulations, in which n elastic degrees of freedom (DOFs) are included to model the structural dynamics, and the number of flight-dynamic equations of mo-

tion (EOMs) increases from the classical six-degree-of-freedom (6-DOF), rigid-body system to a 6+n-DOF system. In this case, one of the greatest advantages of the assumption of small deformations is the possibility of using modal superposition with a small quantity of normal modes retained in the model [1, 5, 6, 7], leading to significantly lower computational cost of numerical simulations than when compared with geometrically-nonlinear models.

Slightly-flexible aircraft flight-dynamic models based on small deformations have also been subjected to experimental validation. Silvestre and Luckner [8] demonstrated the applicability of a dynamically-coupled, linearized mean-axis formulation [7] for flight control law and aircraft design, based on favorable comparisons between simulation and flight-test data obtained with a prototype of the utility aircraft Stemme S15.

A relevant theoretical topic in the flight dynamics of flexible aircraft regards the set of constraints that define the body axes. The introduction of n additional structural-dynamic DOFs while keeping the classical six DOFs of the rigid body implies that constraints must be included to eliminate the rigid-body DOFs of the structural-dynamic model. Such constraints are usually expressed by the choice of body axes. Milne [9] delimited three particular choices of body axes: attached, mean and principal axes. In Ref. [5], Milne's concept of attached axes was extended to a more general form named dually-constrained axes, in which the origin of the structural axes (the support point, where elastic deformations are assumed null) does not necessarily coincide with the origin of the flight-dynamic body axes (with respect to which the EOMs are written). In Ref. [1], the generalization was extended with the separation between the body reference frame (BRF) used for the EOMs and an aerodynamic reference frame (ARF) used for calculating aerodynamic loads, which made the methodology described in the initial paragraphs possible.

All the aforementioned dynamically-coupled formulations are adequate whenever large deformations do not occur. This is not the case for very flexible aircraft. An accident with NASA's Helios Prototype HP03-2 on June 26, 2003 served as an unfortunate demonstration of the importance of adequately modeling the nonlinear behavior of very flexible aircraft [10]. Actually, theoretical work in the field was already being carried out at the time. Patil, Hodges and Cesnik [11] developed a nonlinear formulation for the aeroelastic analysis of aircraft in subsonic flow, with a geometrically-exact, nonlinear intrinsic formulation for the beam dynamics in a moving frame [12]. The same authors [13] extended the formulation for the flight dynamics of HALE aircraft.

Cesnik and Brown [14] developed a strain-based formulation for aeroelastically-tailored flexible wings. In Ref. [15], the authors refined their formulation to consider six rigid-body DOFs and fully-coupled three-dimensional bending, twisting, and extensional nonlinear deformation in the beam model. Whereas in Refs. [14, 15] the fuselage and the tail were modeled as rigid, in Ref. [16] Cesnik and Su dealt with a fully-flexible aircraft with slender bodies.

Shearer and Cesnik [17] coupled the 6-DOF EOMs of a reference point on a very flexible aircraft with the low-order constant strain-based nonlinear structural model of Ref. [15]. The formulation was implemented in the University of Michigan's nonlinear aeroelastic simulation toolbox (NAST or UM/NAST).

The development of the remotely-piloted X-HALE [18] aircraft at the University of Michigan deserves mention. As a low-cost platform for nonlinear aeroelastic flight tests and nonlinear control law studies, it aims at capturing interactions not easily obtained or not even possible in wind tunnel tests. The aircraft in its slightly-flexible configuration (aspect ratio of twenty, $AR = 20$) is currently in operation also at ITA in Brazil, and a more flexible configuration ($AR = 30$) will enter into operation in the near future.

In the present paper, the methodology to assess the assumption of small deformations proposed in Ref. [1] is applied to the X-HALE in its four-, six-, and eight-meter-span configurations ($AR = 20$, $AR = 30$, and $AR = 40$, respectively). Results obtained with a linear structural-dynamic, nonlinear flight-dynamic model us-

ing the described methodology are compared with the results obtained with a fully nonlinear model, comprising a geometrically-exact beam formulation [14, 17, 19, 20], implemented in the ITA/AeroFlex program [21, 22]. The aerodynamic model for the undeformed aircraft is the same between both models, based on Hedman's vortex-lattice method (VLM) [23], but only in the geometrically-nonlinear case the aerodynamic mesh is updated to match the instantaneous bending deformation.

Previously obtained results [2] showed that a geometrically-linear formulation can be used with little loss of accuracy for the aircraft with $AR = 20$, and that a geometrically-nonlinear formulation must be used for $AR = 40$. However, the transition between small and large deformations, in the configuration with $AR = 30$, was not sufficiently explored with only equilibrium conditions and small-disturbance analyses. Rather, time-marching simulations become indispensable for the assessment of the validity of the assumption of small deformations, as transient conditions may attain geometrical nonlinearities in spite of an initial condition of small deformations.

This paper then aims at extending these previous works [1, 2] with the inclusion of newly-obtained results from time-marching simulations. Qualitatively, the conclusions are analogous to the ones previously drawn. However, quantitative criteria for evaluating the assumption of small deformations are derived.

2 Theoretical Background

In this paper, a geometrically-linear (GL) formulation for the flight dynamics of flexible aircraft is compared with a geometrically-nonlinear (GN) one. Both are derived from first principles but independently from each other. The subsections that follow describe the most relevant details of the formulations.

2.1 Geometrically-Linear Formulation

The formulation for small deformations is based on Ref. [1]. There, the EOMs for the flexible aircraft were derived using Lagrange's equations, with the elected set of $6+n$ generalized coordinates comprising: the components of the position vector $\mathbf{R}_{O,b}$ of the origin O of a body reference frame (BRF) expressed in the body axes, b; the Euler angles providing the orientation of the BRF with respect to the flat-Earth inertial reference frame (IRF): ψ, θ, and ϕ; and n elastic DOFs of the aircraft structure, constituting the displacement vector $\mathbf{u}_G = \begin{Bmatrix} u_1 & u_2 & \cdots & u_n \end{Bmatrix}^T$.

A structural-dynamic FEM model of the aircraft with lumped properties of inertia is considered available. The transformation matrix $\mathbf{C}_{b0}$ from the inertial frame to the body frame is obtained by a classical sequence (3-2-1) of Euler rotations, ψ, θ and ϕ [24]. Based on such considerations, the kinetic, elastic strain and gravitational potential energies can be calculated as shown in Ref. [2]. Structural dissipation due to damping forces of viscous nature is assumed [25], giving rise to Rayleigh's dissipation function.

The energy expressions and the dissipation function are used in Lagrange's equations for generalized coordinates to obtain the left-hand side of the EOMs. The right-hand side consists of the generalized forces, comprising aerodynamic and propulsive loads. The former are calculated considering the use of the VLM [23], whereas the latter are modeled as concentrated forces acting on the thrust center of each of the engines [2]. The EOMs for the flexible aircraft can be derived with the assumption that no change in aircraft mass occurs with time and are given by [2]:

$$\begin{aligned} &m\dot{\mathbf{V}}_b + m\widetilde{\boldsymbol{\omega}}_b\mathbf{V}_b - m\widetilde{\mathbf{s}_{CG,b}}\dot{\boldsymbol{\omega}}_b - m\widetilde{\boldsymbol{\omega}}_b\widetilde{\mathbf{s}_{CG,b}}\boldsymbol{\omega}_b \\ &\quad + m\dot{\widetilde{\boldsymbol{\omega}}}_b\mathbf{D}_{CG,b}\mathbf{u}_G + 2m\widetilde{\boldsymbol{\omega}}_b\mathbf{D}_{CG,b}\dot{\mathbf{u}}_G \\ &+ m\widetilde{\boldsymbol{\omega}}_b\widetilde{\boldsymbol{\omega}}_b\mathbf{D}_{CG,b}\mathbf{u}_G + m\mathbf{D}_{CG,b}\ddot{\mathbf{u}}_G = m\mathbf{g}_b + \mathbf{F}_b + \Delta\mathbf{F}_b, \end{aligned} \tag{1}$$

$$\begin{aligned} &\mathbf{J}_O\dot{\boldsymbol{\omega}}_b + \widetilde{\boldsymbol{\omega}}_b\mathbf{J}_O\boldsymbol{\omega}_b + m\widetilde{\mathbf{s}_{CG,b}}\left(\dot{\mathbf{V}}_b + \widetilde{\boldsymbol{\omega}}_b\mathbf{V}_b\right) \\ &\quad + m\widetilde{\mathbf{D}_{CG,b}\mathbf{u}_G}\left(\dot{\mathbf{V}}_b + \widetilde{\boldsymbol{\omega}}_b\mathbf{V}_b\right) \\ &\quad + \Delta\mathbf{J}'_O\dot{\boldsymbol{\omega}}_b + \widetilde{\boldsymbol{\omega}}_b\Delta\mathbf{J}'_O\boldsymbol{\omega}_b + \Delta\dot{\mathbf{J}}'_O\boldsymbol{\omega}_b \\ &\quad + \dot{\mathbf{M}}_{\boldsymbol{\omega}G}\dot{\mathbf{u}}_G + \mathbf{M}_{\boldsymbol{\omega}G}\ddot{\mathbf{u}}_G + \widetilde{\boldsymbol{\omega}}_b\mathbf{M}_{\boldsymbol{\omega}G}\dot{\mathbf{u}}_G \\ &= m\widetilde{\mathbf{s}_{CG,b}}\mathbf{g}_b + m\widetilde{\mathbf{D}_{CG,b}\mathbf{u}_G}\mathbf{g}_b + \mathbf{M}_{O,b} + \Delta\mathbf{M}_{O,b}, \end{aligned} \tag{2}$$

$$\begin{aligned}&\mathbf{M}_{GG}\ddot{\mathbf{u}}_G+\mathbf{B}_{GG}\dot{\mathbf{u}}_G+\mathbf{K}_{GG}\mathbf{u}_G\\&+m\mathbf{D}_{CG,b}{}^T\left(\dot{\mathbf{V}}_b+\widetilde{\boldsymbol{\omega}_b}\mathbf{V}_b\right)+\mathbf{M}_{\boldsymbol{\omega}G}{}^T\dot{\boldsymbol{\omega}}_b\\&+2\dot{\mathbf{M}}^T_{\boldsymbol{\omega}G}\boldsymbol{\omega}_b-\frac{1}{2}\sum_{g=1}^{n}\mathbf{e}_{n,g}\boldsymbol{\omega}_b{}^T\frac{\partial\Delta\mathbf{J}_O}{\partial u_g}\boldsymbol{\omega}_b\\&=m\mathbf{D}_{CG,b}{}^T\mathbf{g}_b+\mathbf{Q}_G.\end{aligned}\tag{3}$$

In Eqs. (1)-(3), $\boldsymbol{\omega}_b=\begin{Bmatrix}p & q & r\end{Bmatrix}^T$ is the angular velocity vector of the BRF with respect to the IRF; $\mathbf{V}_b=\begin{Bmatrix}u & v & w\end{Bmatrix}^T$ is the velocity vector of the BRF origin O with respect to the IRF; the skew-symmetric operator, $\widetilde{(\bullet)}$ or skew $(\bullet)$, denotes the matrix-form of the vector cross product; m is the aircraft total mass; $\mathbf{s}_{CG,b}$ refers to the CG position vector in the undeformed (unstrained) condition; $\mathbf{d}_{CG,b}=\mathbf{D}_{CG,b}\mathbf{u}_G$ stands for the change in $\mathbf{s}_{CG,b}$ due to structural deformation; $\mathbf{J}_O$ is the inertia matrix about O; $\Delta\mathbf{J}'_O$ is the change in the inertia matrix due to structural deformation; $\mathbf{M}_{GG}$, $\mathbf{B}_{GG}$, and $\mathbf{K}_{GG}$ are the FEM mass, damping and stiffness matrices, respectively; $\mathbf{F}_b$ and $\mathbf{M}_{O,b}$ are the net force and moment vectors, respectively, associated with the rigid airframe; $\Delta\mathbf{F}_b$ and $\Delta\mathbf{M}_{O,b}$ are the net incremental force and moment vectors, respectively, due to elastic motion; $\mathbf{g}_b$ is the gravity vector expressed in the BRF; $\mathbf{Q}_G$ is the column matrix of generalized aerodynamic and propulsive forces; at last, $\mathbf{M}_{\boldsymbol{\omega}G}$ is the inertia coupling matrix between the rotational rigid-body and the elastic DOFs. The total number of elastic DOFs is n. The notation $\mathbf{e}_{N,i}$ represents a column matrix equal to the ith column of the identity matrix of order N, $\mathbf{I}_N$. All time derivatives are taken in the BRF.

2.1.1 *Dually-Constrained Axes*

The FEM stiffness matrix, $\mathbf{K}_{GG}$, refers to an unrestrained 3D structure and hence it is a positive semi-definite matrix, with a null space spanned by six linearly-independent vectors [26]. In other words, six linearly-independent rigid-body motions are allowed by this FEM formulation. This rigid-body freedom of the FEM model is not desired, since the coordinates of the origin O and the Euler angles were already considered to be the rigid-body DOFs of the flexible aircraft. This means that six constraints are needed to eliminate the rigid-body motion from the elastic DOFs.

In the present paper, the so-called dually-constrained axes (DCA) [1] are used to constrain the six redundant DOFs. In the DCA, the origin S of the structural axes (the support point, with no elastic displacement) is a material point (and structural node) that can be non-coincident with the origin O of the body axes. Details of the constraint equations of the DCA can be found in Refs. [1, 2]. Any structural node can have its displacements assumed null in the formulation, and the origin O keeps its position constant with respect to the undeformed aircraft (first constraint) and the structural node S is the point where the undeformed and the deformed airframes coincide at any time instant (second constraint).

2.1.2 *Aerodynamic Model*

The aerodynamic loads acting on the flexible aircraft are the superposition of loads that would be obtained were the airframe rigid with incremental loads due to structural deformation. In this paper, the generalized aerodynamic loads are calculated with the VLM [23], which provides the following linear system of equations:

$$\mathbf{A}^{-1}\Delta\mathbf{C}_\mathbf{p}=\mathbf{w},\tag{4}$$

where $\mathbf{w}\in\mathbb{R}^{N_P}$ is the vector of non-dimensional normalwashes at the N_P panel (box) control points; $\Delta\mathbf{C}_\mathbf{p}\in\mathbb{R}^{N_P}$ is the vector of panel pressure coefficient differences; and $\mathbf{A}\in\mathbb{R}^{N_P\times N_P}$ is the AIC (aerodynamic influence coefficient) matrix. The VLM AIC matrix depends on the geometry and discretization of the aerodynamic lifting surfaces in the model. Dependence on the Mach number, M, is neglected in this paper.

The body frame of reference used to calculate the aerodynamic loads is defined as an aerodynamic reference frame (ARF) [1]. Its inertial angular rates are written in the ARF coordinate system as p_a, q_a, and r_a, and its inertial velocity has the components u_a, v_a, and w_a in the same system [1]. The rigid-body motion of the aircraft then contributes to the generalized aerodynamic forces (GAFs) in the elastic DOFs in terms of p_a,

q_a, r_a, u_a, v_a, w_a, control surface deflections and other possible rigid-body variables. The elastic deformation of the structure with respect to the ARF, given by $\mathbf{u}_{G/A}$, contributes to the incremental GAFs. The total GAFs are then given by [1]:

$$\mathbf{Q}_G = \bar{q}\mathbf{G}_{AG}{}^T\mathbf{S}_{AP}\left(\Delta\mathbf{C}_{\mathbf{p},\mathbf{u}} + \Delta\mathbf{C}_{\mathbf{p},\mathbf{e}}\right), \quad (5)$$

where $\bar{q}$ is the dynamic pressure; $\mathbf{G}_{AG} \in \mathbb{R}^{N_A \times n}$ is the matrix that interpolates elastic displacements from the structural nodes to the centroids of the VLM boxes (aerodynamic grid points); $\mathbf{S}_{AP} \in \mathbb{R}^{N_A \times N_P}$ transforms panel pressure coefficient differences to forces and moments at the aerodynamic grid points, and is usually called an integration matrix; $\Delta\mathbf{C}_{\mathbf{p},\mathbf{u}}$ is the vector of panel pressure coefficient differences related to the rigid-body state and control variables; and $\Delta\mathbf{C}_{\mathbf{p},\mathbf{e}}$ is the vector of panel incremental pressure coefficient differences, due to the elastic DOFs, given by [1]:

$$\Delta\mathbf{C}_{\mathbf{p},\mathbf{e}} = \mathbf{A}\left(\mathbf{D}_{PA,0}\mathbf{G}_{AG}\mathbf{u}_{G/A} + (b_w/V_a)\,\mathbf{D}_{PA,1}\mathbf{G}_{AG}\dot{\mathbf{u}}_{G/A}\right), \quad (6)$$

where $\mathbf{D}_{PA,0}, \mathbf{D}_{PA,1} \in \mathbb{R}^{N_P \times N_A}$ are the differentiation matrices that allow the calculation of control point normalwashes at three quarters of the boxes' mean chords from the displacements at the aerodynamic grid points, respectively; b_w is the reference wing semi-chord; and $N_A = 2N_P$ is the total number of aerodynamic degrees of freedom (each panel has two DOFs, plunge and pitch). The integration and differentiation matrices in Eqs. (5)-(6) can be found in Ref. [2].

In this paper, the ARF is modeled with attached axes [1]. Hence, their origin A coincides with or is rigidly connected to a material point C that remains fixed when elastic deformation occurs. References [1, 2] present the equations for the aerodynamic loads based on the ARF DOFs. Induced drag effects due to both the rigid-body motion and the elastic deformation are included, calculated with the methodology of Ref. [27].

2.1.3 *Geometrically-linear beam elements*

The adopted geometrically-linear beam element in three dimensions has two nodes and twelve DOFs. The element shape functions are given by:

$$u_e(x_e,y_e,z_e) = a_0 + a_1 x_e - \frac{\partial w_e}{\partial x_e} z_e - \frac{\partial v_e}{\partial x_e} y_e, \quad (7)$$

$$v_e(x_e,y_e,z_e) = \sum_{i=0}^{3} b_i {x_e}^i - \Theta_e(x_e,y_e,z_e)\, z_e, \quad (8)$$

$$w_e(x_e,y_e,z_e) = \sum_{i=0}^{3} c_i {x_e}^i + \Theta_e(x_e,y_e,z_e)\, y_e, \quad (9)$$

where $u_e(x_e,y_e,z_e)$ is the axial displacement and $v_e(x_e,y_e,z_e)$ and $w_e(x_e,y_e,z_e)$ are the edgewise and flatwise displacements' shape functions, respectively. The set becomes complete with the twist angle shape function:

$$\Theta_e(x_e,y_e,z_e) = d_0 + d_1 x_e. \quad (10)$$

The twelve DOFs of the beam element are, at $x_e = y_e = z_e = 0$: $u_e = u_{e1}$, $v_e = v_{e1}$, $w_e = w_{e1}$, $\Theta_e = \phi_{e1}$, $\frac{\partial w_e}{\partial x_e} = -\theta_{e1}$, $\frac{\partial v_e}{\partial x_e} = \psi_{e1}$; at $x_e = L_e, y_e = z_e = 0$: $u_e = u_{e2}$, $v_e = v_{e2}$, $w_e = w_{e2}$, $\Theta_e = \phi_{e2}$, $\frac{\partial w_e}{\partial x_e} = -\theta_{e2}$, and $\frac{\partial v_e}{\partial x_e} = \psi_{e2}$, where L_e is the element length. Strains are given by:

$$\varepsilon_x = \frac{\partial u_e}{x_e}, \quad (11)$$

$$\varepsilon_y = -\nu\varepsilon_x, \quad (12)$$

$$\varepsilon_z = -\nu\varepsilon_x, \quad (13)$$

$$\gamma_{xy} = \frac{\partial v_e}{x_e} + \frac{\partial u_e}{y_e}, \quad (14)$$

$$\gamma_{xz} = \frac{\partial w_e}{x_e} + \frac{\partial u_e}{z_e}, \quad (15)$$

$$\gamma_{yz} = \frac{\partial w_e}{y_e} + \frac{\partial v_e}{z_e}, \quad (16)$$

where ν is the material Poisson's ratio. Using Voigt's notation, the element strains may be collected in a six-dimensional column matrix, $\boldsymbol{\varepsilon} = \{\varepsilon_x \;\; \varepsilon_y \;\; \varepsilon_z \;\; \gamma_{xy} \;\; \gamma_{xz} \;\; \gamma_{yz}\}^T$, which is itself a linear function of the twelve element DOFs. Stresses can be calculated with consideration of the isotropic linear elastic material stiffness matrix, $\mathbf{C}$, presented in Ref. [2], so that:

$$\boldsymbol{\sigma} = \mathbf{C}\boldsymbol{\varepsilon}. \quad (17)$$

The element stiffness matrix $\mathbf{K}_{ee}$ is such that the element strain energy satisfies:

$$U_e = \frac{1}{2}\iiint_{element} \boldsymbol{\sigma}^T \boldsymbol{\varepsilon} dV = \frac{1}{2}\mathbf{u}_e{}^T \mathbf{K}_{ee}\mathbf{u}_e, \tag{18}$$

with $\mathbf{u}_e = \{u_{e1} \;\; v_{e1} \;\; w_{e1} \;\; \phi_{e1} \;\; \theta_{e1} \;\; \psi_{e1} \;\; u_{e2} \;\; v_{e2} \;\; w_{e2} \;\; \phi_{e2} \;\; \theta_{e2} \;\; \psi_{e2}\}^T$. The final equation for the stiffness matrix is presented in Ref. [2] and is omitted here for brevity.

Although a consistent mass matrix can also be obtained for the beam element, the flight-dynamic formulation is not prepared to deal with consistent masses, due to resulting inertial coupling between the two element nodes. Rather, a lumped mass matrix is generated by transferring to each node half of the mass of the element, as well as the first and second moments of inertia and the products of inertia due to each half.

2.2 Strain-based geometrically-nonlinear beam formulation

In this paper, the strain-based geometrically-nonlinear (GN) formulation is based on Refs. [19, 20, 28, 29]. A toolbox named ITA/AeroFlex was developed with this formulation, using MATLAB® [22]. The formulation considers the following fundamental kinematic relationship that relates the displacements $h(s,t)$ at a point along the beam to the strains $\varepsilon(s,t)$:

$$\frac{\partial h}{\partial s}(s,t) = \mathcal{K}(s,t)h(s,t), \tag{19}$$

$$\mathcal{K}(s,t) = \tag{20}$$
$$= \begin{bmatrix} 0 & 1+\varepsilon_x(s,t) & 0 & 0 \\ 0 & 0 & \kappa_z(s,t) & -\kappa_y(s,t) \\ 0 & -\kappa_z(s,t) & 0 & \kappa_x(s,t) \\ 0 & \kappa_y(s,t) & -\kappa_x(s,t) & 0 \end{bmatrix},$$

where $\varepsilon_x(s,t)$ is the extensional strain, and $\kappa_x(s,t)$, $\kappa_y(s,t)$ and $\kappa_z(s,t)$ are the curvatures at point s and time t.

The flexible structure is split into elements and the strains are assumed to be spatially-constant but time-dependent along each element, so that Eq. 19 has an analytical solution:

$$h(s,t) = e^{\mathcal{K}(s-s_0)}h_0(t), \tag{21}$$

where $h_0(t)$ is the displacement of a fixed node at $s = s_0$. The matrix exponential $e^{\mathcal{K}(s-s_0)}$ has a closed-form expression as presented in Ref. [20].

In the ITA/AeroFlex computer program, flexible elements with three nodes were implemented, as well as rigid elements with time-independent, null strain. Such rigid elements are used to model rigid components and do not introduce new states to the model.

Using Eq. 21, it is possible to compute the displacement vector for each structural node as a function of the strains:

$$h(t) = h\left(\varepsilon(t)\right). \tag{22}$$

The time derivative of the displacement vector due to both the strain rates $\dot{\varepsilon}$ and the rigid-body motion β (linear and angular velocity components) is given by:

$$\dot{h}(t) = J_{h\varepsilon}\dot{\varepsilon}(t) + J_{hb}\beta(t). \tag{23}$$

where $J_{h\varepsilon}(\varepsilon(t))$ is a Jacobian that relates the element strains to nodal displacements and J_{hb} is the equivalent but for the rigid-body motion.

The kinetic energy is computed as:

$$T = \frac{1}{2}\dot{h}^T M \dot{h}, \tag{24}$$

where M is the structure mass matrix, computed assuming a linear variation of the nodal speeds between the nodes. The kinetic energy can be rewritten as a function of the strain rates and rigid-body velocities using Eq. 23:

$$T = \frac{1}{2}\begin{bmatrix}\dot{\varepsilon} & \beta\end{bmatrix}\begin{bmatrix} M_{FF} & M_{FB} \\ M_{BF} & M_{BB}\end{bmatrix}\begin{bmatrix}\dot{\varepsilon} \\ \beta\end{bmatrix}, \tag{25}$$

where:

$$\begin{aligned} M_{FF} &= J_{h\varepsilon}^T M J_{h\varepsilon}, \quad M_{FB} = J_{h\varepsilon}^T M J_{hb}, \\ M_{BF} &= J_{hb}^T M J_{h\varepsilon}, \quad M_{BB} = J_{hb}^T M J_{hb}. \end{aligned} \tag{26}$$

The elastic strain energy is given by:

$$U = \frac{1}{2}\varepsilon^T K \varepsilon, \tag{27}$$

where K is a block-diagonal matrix, composed of the stiffness matrices of each element, K^e:

$$K^e = \begin{bmatrix} k_{11} & k_{12} & k_{13} & k_{14} \\ k_{21} & k_{22} & k_{23} & k_{24} \\ k_{31} & k_{32} & k_{33} & k_{34} \\ k_{41} & k_{42} & k_{43} & k_{44} \end{bmatrix}. \tag{28}$$

From the Euler-Lagrange equations, the equations of motion are computed as:

$$\begin{bmatrix} M_{FF} & M_{FB} \\ M_{BF} & M_{BB} \end{bmatrix} \begin{bmatrix} \ddot{\varepsilon} \\ \dot{\beta} \end{bmatrix} + \begin{bmatrix} C_{FF} & C_{FB} \\ C_{BF} & C_{BB} \end{bmatrix} \begin{bmatrix} \dot{\varepsilon} \\ \beta \end{bmatrix} + \begin{bmatrix} K \\ 0 \end{bmatrix} \varepsilon = \begin{bmatrix} R_F \\ R_B \end{bmatrix} \tag{29}$$

The matrices C_{FF}, C_{BF}, C_{FB} and C_{BB} include the gyroscopic terms (due to rotation of the rigid body and of the structural elements) and the structural damping term. In this paper, the structural damping matrix is assumed proportional to the stiffness matrix: $C_{FF} = \alpha K$.

R_F and R_B are the generalized forces that are applied to the airplane. They are obtained from the aerodynamic, gravitational and propulsive forces applied to each node of the structure:

$$\begin{bmatrix} R_F \\ R_B \end{bmatrix} = \begin{bmatrix} J_{p\varepsilon}^T \\ J_{pb}^T \end{bmatrix} F^{pt} + \begin{bmatrix} J_{\theta\varepsilon}^T \\ J_{\theta b}^T \end{bmatrix} M^{pt} + \begin{bmatrix} J_{p\varepsilon}^T \\ J_{pb}^T \end{bmatrix} B^F F^{dist} + \begin{bmatrix} J_{\theta\varepsilon}^T \\ J_{\theta b}^T \end{bmatrix} B^F M^{dist} + \begin{bmatrix} J_{p\varepsilon}^T \\ J_{pb}^T \end{bmatrix} N\vec{g} \tag{30}$$

The Jacobian matrices $J_{p\varepsilon}$ and $J_{\theta\varepsilon}$ represent the relationship between structural strains (ε) and nodal displacements and rotations. J_{pb} and $J_{\theta b}$ represent the relationship between rigid-body DOFs and nodal displacements and rotations. The Jacobian matrices are nonlinear functions of the strain vector ε. Closed-form expressions for the Jacobians are presented in [20].

3 Numerical Models

The X-HALE aircraft in its four- ('XH4'), six- ('XH6') and eight-meter-span ('XH8') configurations is analyzed. The XH4 configuration contains four wing sections with span of 1.0 m and chord of 0.2 m each, as well as three pods at the connections between wing sections. The aircraft engines, landing gears, electronics and sensors are installed at the pods. Booms are connected to the pods and, at the tip of each boom, a horizontal tail is mounted. The two side tails are all-moving control surfaces that can be used for both longitudinal and lateral-directional control, and are then termed elevons. The central tail has a flipping-up capability that alters the aircraft flying qualities as desired in operation. For ground clearance during take-off, the central tail has approximately 33% less span in its right (bottom) part than in the left (top) part. Anyway, all configurations analyzed in this paper have the central tail in the horizontal position. The wing-tip sections have a dihedral angle of 10°. The wing is built with an incidence of 5°.

The XH6 configuration has two more wing sections, pods, booms and tails than the XH4. The XH8 configuration has only two wing sections added with respect to the XH6 configuration, without additional pods, booms or tails.

The numerical models consider exactly the same stiffness properties previously adopted in Ref. [2], and these properties are employed in both the GL and the GN formulations. All aircraft components except the wing are assumed rigid. The distributed mass properties of the aircraft components are also identical to those presented in Table 1 of Ref. [2]. The concentrated inertias match those listed in Table 7 of Ref. [18].

3.1 Verification of the models

The focus of this paper is on time-marching simulations using both the GL and the GN formulations. Because all structural DOFs are kept in the EOMs for both formulations, the resulting dynamical systems have hundreds of states and the differential equations are stiff. Having this in mind, the criterion used to create the structural-dynamic models in this paper is different from the one used previously in Ref. [2], where the authors were concerned almost only with accuracy of the models in static conditions, with model size having less computational impact because differential equations were not to be solved. Con-

vergence analyses led to 10 elements per wing section in the GN formulation and of 20 in the GL one in Ref. [2]. With such choices, the wing had the same quantity of nodes in both models.

However, numerical tests demonstrated that simulations using such refinement would be unfeasible using the current routines implemented in the ITA/AeroFlex program. Because the differential equations are stiff, common solvers do not work for the GL or the GN simulations. Rather, it was found that the generalized-α algorithm [30, 31, 20] was able to solve the equations. Currently, the nonlinear balance equation of this implicit algorithm is solved at each time step with the trust-region dogleg algorithm implemented in the MATLAB® 'fsolve' function. A reduction in the number of structural DOFs was then mandatory to make the simulations less costly and the present work feasible.

It was found that using 4 elements per wing section in the GN model and 8 elements in the GL yields no more than 3.5% difference between them in modal frequencies less than 20 Hz for the XH6 configuration. This refinement can be considered enough for the purpose of the present paper, which is to identify when nonlinearities start to play an important physical role in the flight dynamics of flexible aircraft, in phenomena that are much likely to occur at lower frequencies. Moreover, a time step of 10 milliseconds is used in the generalized-α method, rendering differences in higher-frequency modes progressively less important the farther they are from 20 Hz.

The VLM mesh is the same for both formulations and, for the same reasons as the aforementioned ones, is coarser than the one adopted in Ref. [2]. For simplicity, it was built to match the spanwise divisions of the wing sections in the GN structural-dynamic model, that is, it comprises 4 uniformly distributed boxes spanwise per wing section. Chordwise, 4 boxes are used in the wing, also uniformly distributed. The tails are divided into 2 boxes chordwise and 2 boxes spanwise. No vertical surface representing each pod is included in the aerodynamic model, also for simplicity.

The wing incidence of 5° and the wing reflexed EMX07 airfoil [18] camber are approximately represented by invariant normalwash vectors, given by the local effective camber line inclination at 75% of each box chord.

In the GN formulation, the VLM mesh is updated with structural deformation, such that the wing and tails' boxes' side edges are displaced both laterally and vertically by exactly the same amount as the structural node with which they coincide spanwise. Hence, the mesh update makes the aerodynamic forces consistently behave as follower forces in the GN formulation.

The displacements and displacement rates of the beam elements' central nodes in the GN formulation are directly used to calculate the normalwashes. No camber deformation is considered, and hence the displacement transferal from the structural nodes to the boxes' control points is straightforward, assuming rigid arms. The aerodynamic loading is considered as distributed, and appropriate matrices transfer the distributed loads to nodal loads at each element, as in Eq. (30).

In the GL formulation, to preserve linearity, the VLM mesh is never updated. Linear spline interpolation matrices, as derived in Ref. [4], are calculated and used. Guimarães Neto et al. [2] did already validate the aerodynamic model implementations. The GL structural-dynamic model and the VLM mesh are plotted in Figs. 1-2 for the XH6 configuration, with the XH4 and XH8 models being analogous.

4 Numerical Results

Three different support locations are used in the GL formulation. One is at a central location at the wing structural node in the wing symmetry plane, and is denoted 'C'. The two others are at the structural nodes at the wing tips, named 'L' for the left one and 'R' for the right one. Therefore, the plots presented hereinafter will contain three data sets for the GL formulation: GLC, GLL, and GLR. These shall be compared with the single data set obtained with the geometrically-nonlinear implementation: GN.

Stiffness-proportional structural damping is considered, with a constant of proportionality such that the first free-free mode of vibration has

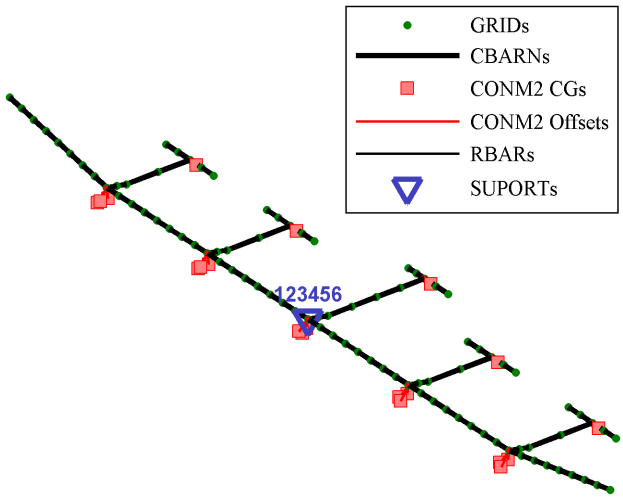

Fig. 1 XH6 GL structural-dynamic model in ITA/AeroFlex. GRIDs: structural nodes; CBARNs: beam elements; RBARs: rigid bar elements; CONM2 CGs: CG locations of lumped-mass elements; CONM2 Offsets: offsets between such CG locations and the structural node to which the lumped-mass element is attached; and SUPORT: support location.

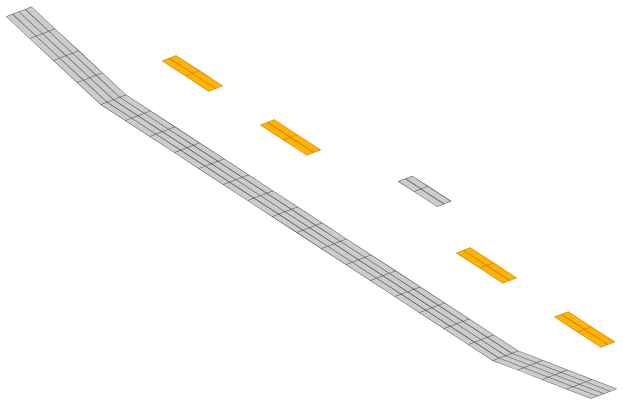

Fig. 2 XH6 configuration VLM model in ITA/AeroFlex. Control surfaces in orange.

2% damping ratio.

The obtained results for equilibrium conditions with the coarser structural-dynamic and aerodynamic models are similar to the results previously obtained with the more refined ones in Ref. [2]. However, it was now possible to calculate trimmed conditions in a longitudinal maneuver with vertical load factor of 2. Table 1 and Figs. 3-5 show the results in terms of structural deformations. The deformations for the GL formulation are with respect to a common ARF.

	Wing Tip	Displacements [m]		
		XH4	XH6	XH8
GLL	Left	0.192 (−2.5%)	0.578 (−8.0%)	2.015 (−21.8%)
	Right	0.196 (−1.5%)	0.599 (−5.4%)	2.275 (−11.8%)
GLC	Left	0.197	0.628	2.577
	Right	0.199	0.633	2.580
GLR	Left	0.194 (−1.5%)	0.594 (−5.4%)	2.273 (−11.8%)
	Right	0.194 (−2.5%)	0.583 (−7.9%)	2.017 (−21.8%)
GN	Left	0.221 (+12.2%)	1.018 (+62.1%)	2.345 (−9.0%)
	Right	0.223 (+12.1%)	1.029 (+62.6%)	2.356 (−8.7%)

Table 1 Wing tip vertical displacements (positive upwards) for the X-HALE configurations in trimmed longitudinal flight with a vertical load factor of 2 at 20 m/s. (Percentages with respect to GLC left and right wing tip displacements.)

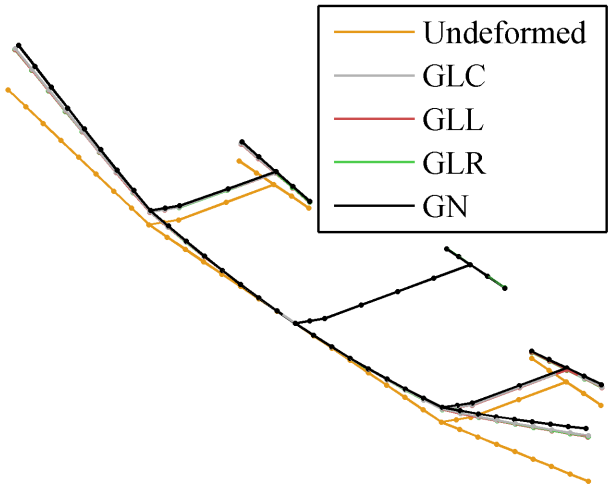

Fig. 3 XH4 configuration in trimmed longitudinal flight with a vertical load factor of 2 at 20 m/s.

Two factors shall be considered when analyzing Table 1 and Figs. 3-5: first, the differences in

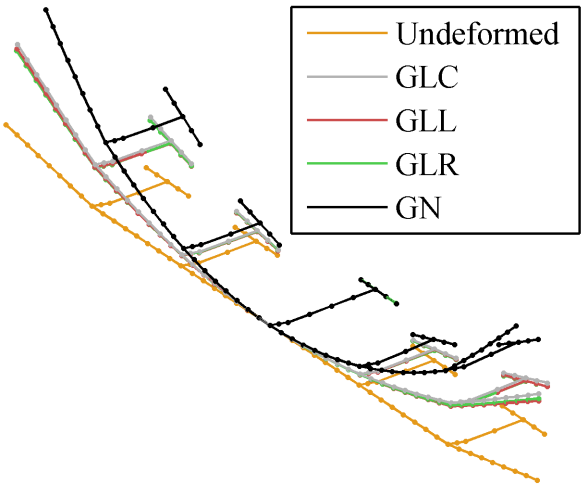

Fig. 4 XH6 configuration in trimmed longitudinal flight with a vertical load factor of 2 at 20 m/s.

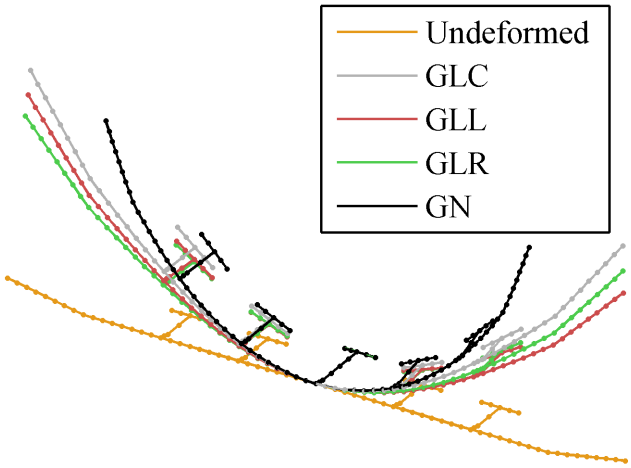

Fig. 5 XH8 configuration in trimmed longitudinal flight with a vertical load factor of 2 at 20 m/s.

structural deformations for different support locations in the GL formulation; second, the fact that the aerodynamic mesh is updated only in the GN formulation. Hence, for the XH4 configuration, one sees that the difference between different support locations is practically negligible; however, the GN result shows a slightly greater deformation, possibly due to the follower-force effect enabled by the mesh update. For the XH6 configuration, differences of up to 8.0% in wing tip displacements are already observed in the GL formulation between the central and wing tip support locations, suggesting the presence of geometrical nonlinearity. This is confirmed by the GN result, which predicts significantly greater structural deformations. It is interesting to observe that the GL formulation predicts wing tip deformation of up to 21.1% of the nominal wing semi-span in this case. The XH8 is clearly highly flexible, with significant differences between the support locations in the GL formulation and strong nonlinearities in the deformed U shape seen in Fig. 5.

Time-marching simulations were performed with commanded elevon doublets. The elevon doublet can be either symmetrical, lasting 0.6 second and applied to all the elevons, or anti-symmetrical, lasting 1.4 second and applied only to the outboard elevons. The doublets have 5.0° amplitude and are C1-continuous with cubic transitions lasting 0.1, 0.2 and 0.1 second, respectively. The commands begin at $t = 0.2$ s, with the aircraft initially in a trimmed level-flight condition. The first pulse is positive for the right elevon(s), and the second is negative.

Figure 6 shows that the pitch rate response of the XH4 configuration to the symmetrical elevon doublet is practically the same for all formulations considered, and the wing tip vertical displacement does not exceed 12% of the wing semi-span. Small deformations can be assumed.

The same is not observed for the XH6 configuration. As seen in Fig. 7, there is disagreement in the pitch rate between the GLL, GLR and GLC formulations, particularly when the wing deformation is near or at its maximum. According to the methodology proposed in Ref. [1], this indicates that geometrical nonlinearities are potentially present. This is confirmed by the plots of the GN formulation, with discrepancies observed in how fast the wing tip recovers its equilibrium deformation. Figure 7 also shows that the wing tip vertical displacement reaches almost 14.7% of the wing semi-span in the GL formulation.

The anti-symmetrical elevon doublet also shows interesting results for the XH6 configuration in Fig. 8. First, elevon roll reversal is observed, as the elevons are initially deflected in a sense that would result in a roll to the left in a rigid aircraft, with the flexible aircraft rolling

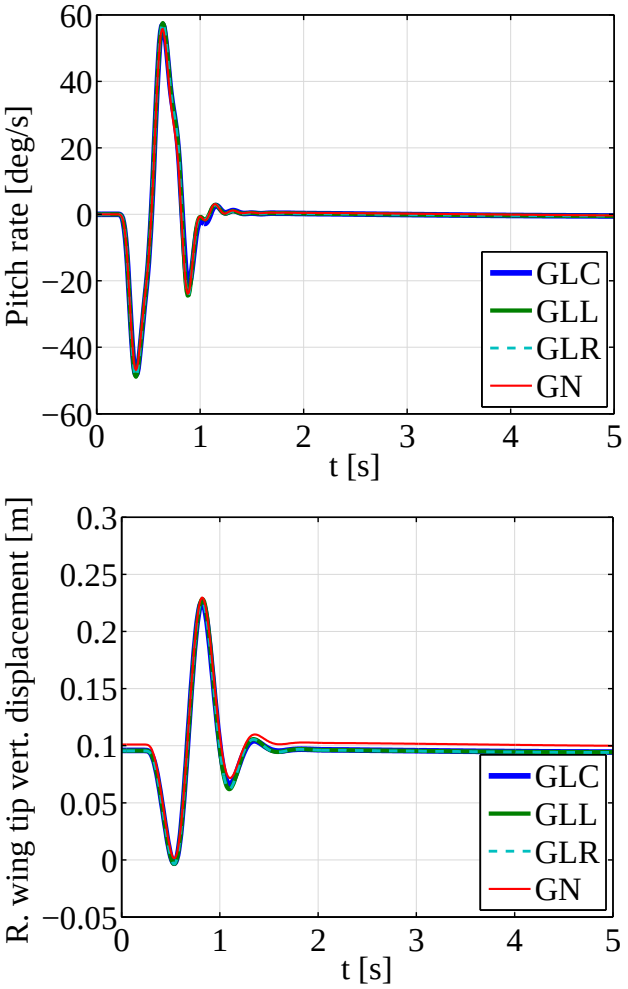

Fig. 6 XH4 response to symmetrical elevon doublet at 20 m/s.

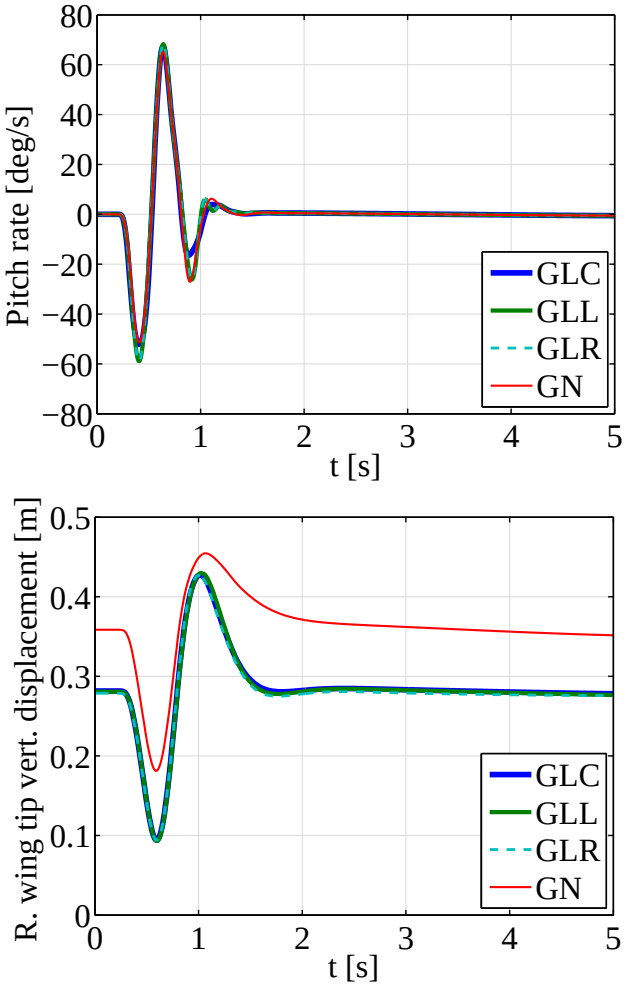

Fig. 7 XH6 response to symmetrical elevon doublet at 20 m/s.

to the right. The wing tip pitch rates are initially positive in the left wing tip and negative in the right one, confirming that significant wing twist produces the reversal. Moreover, geometrical nonlinearities occur, but another important phenomenon is also present: because the lifting surfaces have their boxes' dihedral angles constantly updated in the GN formulation, the aircraft lateral-directional characteristics do not only start different from those of the GL formulation but are constantly changing during the simulation. This explains why the GN formulation attains smaller roll rate in response to the anti-symmetrical elevon doublet.

At last, the results for the symmetrical elevon doublet for the XH8 configuration are presented in Fig. 9. The disagreement in the pitch rate between the GLL, GLR and GLC formulations is much more pronounced during and after the application of the doublet. There is no agreement at all with the GN formulation, demonstrating that geometrically-linear structural dynamics is not applicable to such a highly-flexible aircraft.

5 Conclusions

A self-contained methodology to assess the assumption of small deformations in geometrically-linear structural-dynamic models was applied to aircraft with different levels of structural flexibility. The methodology allegedly does not depend on the availability of higher-fidelity, geometrically-nonlinear models, because it is based on the validity of the linear rigid-body

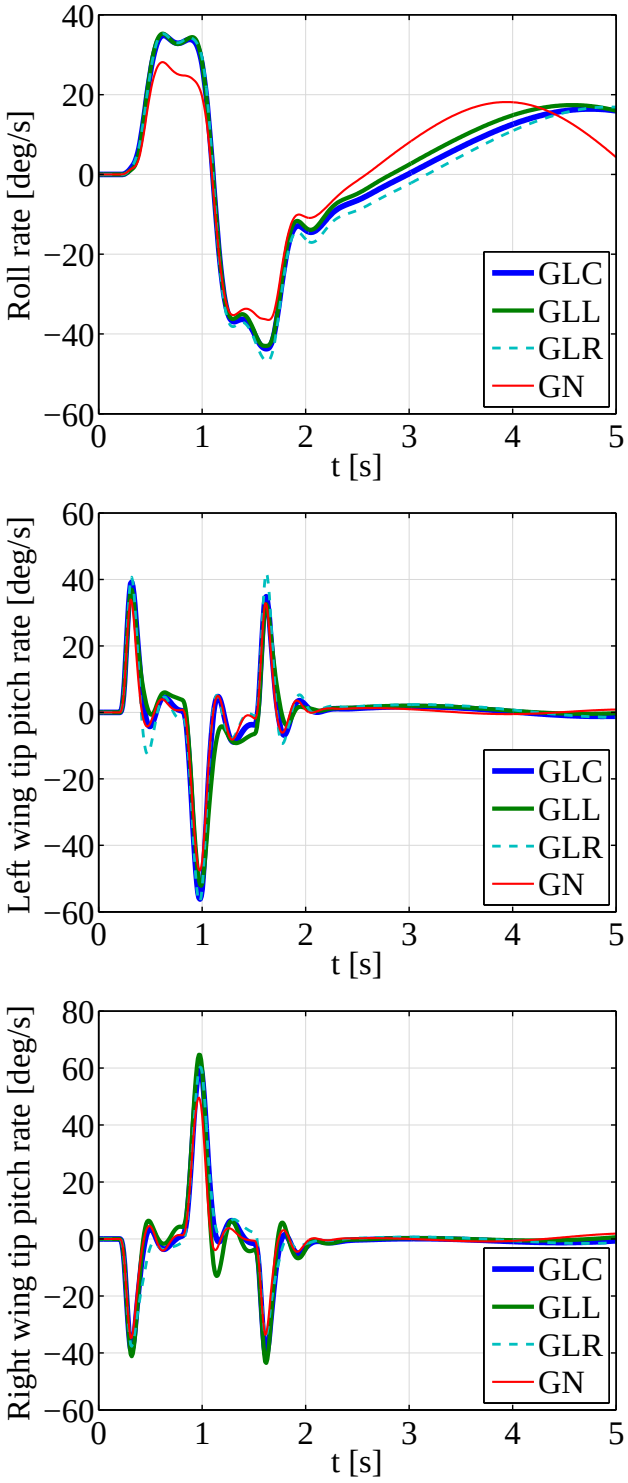

Fig. 8 XH6 response to anti-symmetrical elevon doublet at 20 m/s.

modes of the structure, which, once violated, also implies the violation of the assumption of small deformations.

In order to validate the methodology, however, geometrically-linear models were compared with a geometrically-nonlinear one in this paper. For any given aircraft, the same number of wing nodes and the same undeformed aerodynamic model, based on the quasisteady VLM, were employed for both the geometrically-linear and the geometrically-nonlinear formulations. In the latter, the VLM mesh was consistently updated with structural deformation. It remains to be investigated whether including the aerodynamic mesh update in the former would be worth the higher computing cost implied in recalculating the AIC and spline matrices in each time step.

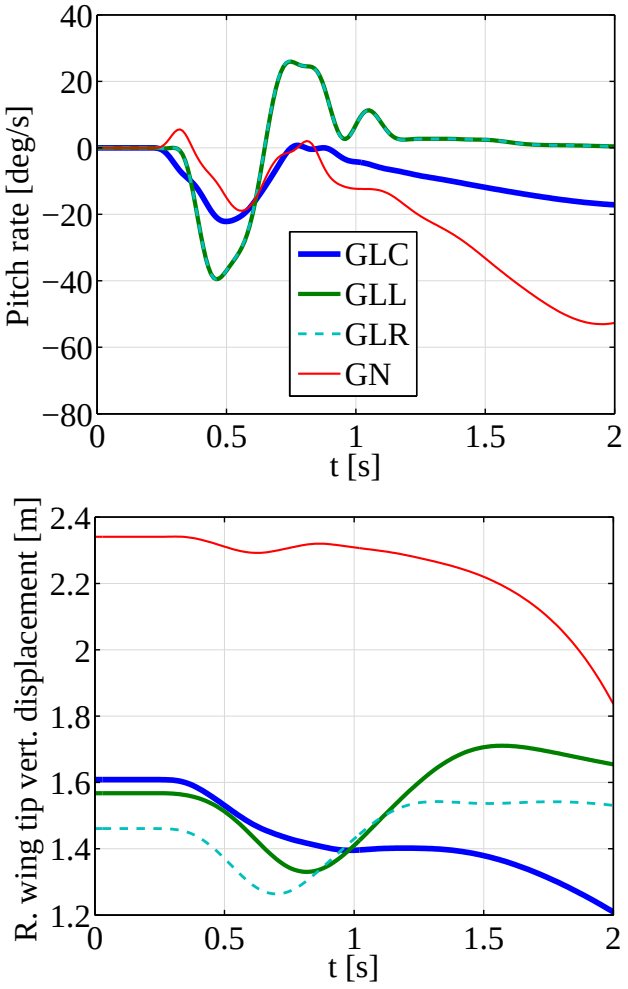

Fig. 9 XH8 response to symmetrical elevon doublet at 14 m/s.

Numerical results indicate that geometrically-linear models do progressively lose fidelity as wing tip displacements exceed 12% of the wing semi-span or relative differences

of more than 5% in any wing tip displacement occur for different support locations. Time-marching simulations also allow us to infer that, if large deformations are attained at some point in time, the aircraft response from that instant on may become unrealistic in geometrically-linear models.

The self-contained methodology has proved its value in that discrepancies in the results for different support locations correspond to disagreements between the geometrically-linear and -nonlinear formulations. Despite structural nodes at the two wing tips were considered as support locations in this paper, the procedure can be directly simplified to consider only one of them. Moreover, aircraft responses in time-marching simulations show that the central support location tends to have the highest correlation with the geometrically-nonlinear formulation.

Contact Author Email Address

antoniobgn@gmail.com

Acknowledgement

This work has been funded by FINEP and EMBRAER under the research project Advanced Studies in Flight Physics, contract number 01.14.0185.00.

Copyright Statement

References

[1] Guimarães Neto, A. B., Silva, R. G. A., Paglione, P. and Silvestre, F. J. Formulation of the flight dynamics of flexible aircraft using general body axes. *AIAA Journal*, Vol. 54, No. 11, pp. 3516-3534, 2016. DOI: 10.2514/1.J054752.

[2] Guimarães Neto, A. B., Silvestre, F. J., Cardoso-Ribeiro, F. L., Bussamra, F. L. S., Silva, R. G. A. and Cesnik. C. E. S. Validity of the assumption of small deformations in aircraft with different levels of structural flexibility. *Proceedings of the International Forum on Aeroelasticity and Structural Dynamics (IFASD)*, Como, Italy, June 25-28, 2017. IFASD-2017-080.

[3] Rodden, W. P. and Love, J. R. Equations of motion of a quasisteady flight vehicle utilizing restrained static aeroelastic characteristics. *Journal of Aircraft*, Vol. 22, No. 9, pp. 802-809, 1985.

[4] Rodden, W. P. and Johnson, E. H. *MSC.NASTRAN Aeroelastic Analysis User's Guide*. MacNeal-Schwendler Corporation, Los Angeles, 1994, Chap. 2.

[5] Guimarães Neto, A. B. *Flight dynamics of flexible aircraft using general body axes:* a theoretical and computational study. Thesis (PhD in Aeronautical and Mechanical Engineering) – Instituto Tecnológico de Aeronáutica, São José dos Campos, Brazil, 2014.

[6] Etkin, B. *Dynamics of flight:* stability and control. John Wiley & Sons, Inc., 1959.

[7] Waszak, M. R. and Schmidt, D. K. Flight dynamics of aeroelastic vehicles. *Journal of Aircraft*, Vol. 25, No. 6, pp. 563-571, 1988.

[8] Silvestre, F. J. and Luckner, R. Experimental validation of a flight simulation model for slightly flexible aircraft. *AIAA Journal*, Vol. 53, No. 12, pp. 3620-3636, 2015. DOI: 10.2514/1.J054023.

[9] Milne, R. D. *Dynamics of the derformable aeroplane*. Her Majesty's Stationary Office TR RM 3345, London, 1964.

[10] Noll, T. E. et al. *Investigation of the Helios prototype aircraft mishap*. Washington, DC: NASA, 2004.

[11] Patil, M. J., Hodges, D. H. and Cesnik, C. E. S. Nonlinear aeroelastic analysis of complete aircraft in subsonic flow. *Journal of Aircraft*, Vol. 37, No. 5, pp. 753-760, 2000.

[12] Hodges, D. H. A mixed variational formulation

based on exact intrinsic equations for dynamics of moving beams. *International Journal of Solids and Structures*, Vol. 26, No. 11, pp. 1253-1273, 1990.

[13] Patil, M. J., Hodges, D. H. and Cesnik, C. E. S. Nonlinear aeroelasticity and flight dynamics of high-altitude long-endurance aircraft. *Journal of Aircraft*, Vol. 38, No. 1, pp. 88-94, 2001.

[14] Cesnik, C. E. S. and Brown, E. L. Modeling of high aspect ratio active flexible wings for roll control. *Proceedings of the 43rd AIAA/ASME/ASCE/AHS/ASC Structures, Structural Dynamics, and materials conference and exhibit*, Denver, 2002. AIAA Paper 2002-1719.

[15] Cesnik, C. E. S. and Brown, E. L. Active wing warping control of a joined-wing airplane configuration. *Proceedings of the 44th AIAA/ASME/ASCE/AHS/ASC Structures, Structural Dynamics, and materials conference and exhibit*, Norfolk, 2003. AIAA Paper 2003-1715.

[16] Cesnik, C. E. S. and Su, W. Nonlinear aeroelastic modeling and analysis of fully flexible aircraft. *Proceedings of the AIAA/ASME/ASCE/AHS/ASC 46th Structures, Structural Dynamics and Materials Conference*, 2005, Austin. AIAA Paper 2005-2169.

[17] Shearer, C. M. and Cesnik, C. E. S. Nonlinear flight dynamics of very flexible aircraft. *Journal of Aircraft*, Vol. 44, No. 5, pp. 1528-1545, 2007.

[18] Cesnik, C. E. S., Senatore, P. J., Su, W., Atkins, E. M. and Shearer, C. M. X-HALE: a very flexible unmanned aerial vehicle for nonlinear aeroelastic aests. *AIAA Journal*, Vol. 50, No. 12, pp. 2820-2833, 2012.

[19] Brown, E. L. *Integrated strain actuation in aircraft with highly flexible composite wings*. Thesis (PhD) – Massachusetts Institute of Technology, 2003.

[20] Shearer, C. M. *Coupled nonlinear flight dynamics, aeroelasticity and control of very flexible aircraft*. Thesis (PhD in Aerospace Engineering) – University of Michigan, Ann Arbor, 2006.

[21] Cardoso-Ribeiro, F. L. *Dinâmica de voo de aeronaves muito flexíveis*. Dissertation (MSc degree in Aeronautical and Mechanical Engineering), Instituto Tecnológico de Aeronáutica, São José dos Campos, Brazil, 2011.

[22] Cardoso-Ribeiro, F. L., Paglione, P., Silva, R. G. A. and Sousa, M. S. AeroFlex: a toolbox for studying the flight dynamics of highly flexible airplanes. *VII Congresso Nacional de Engenharia Mecânica (CONEM)*, São Luís, Maranhão, Brazil, 2012.

[23] Hedman, S. G. *Vortex lattice method for calculation of quasi steady state loadings on thin elastic wings*. Aeronautical Research Inst. of Sweden Rept. 105, Stockholm, 1965.

[24] Stevens, B. L. and Lewis, F. L. *Aircraft control and simulation*. Wiley, Hoboken, NJ, 2003, pp. 25-29; 116-138; 263-265.

[25] Bismarck-Nasr, M. N. *Structural Dynamics in Aeronautical Engineering*. AIAA Education Series, AIAA, Reston, VA, 1999, pp. 53-91.

[26] Mantegazza, P. Tutorial on Attached-Mean Axes and Their Use in the Calculation of Deformable Static and Damped-Undamped Vibration Modes of a Free-Free Structure. *Journal of Aeroelasticity and Structural Dynamics*, Vol. 2, No. 1, pp. 81-98, 2011.

[27] Kálmán, T. P., Giesing, J. P. and Rodden, W. P. Spanwise distribution of induced drag in subsonic flow by the vortex lattice method. *Journal of Aircraft*, Vol. 7, No. 6, pp. 574-576, 1970.

[28] Su, W. *Coupled nonlinear aeroelasticity and flight dynamics of fully flexible aircraft*. Thesis (PhD in Aerospace Engineering) – University of Michigan, Ann Arbor, 2008.

[29] Su, W. and Cesnik, C. E. S. Strain-based geometrically nonlinear beam formulation for modeling very flexible aircraft. *International Journal of Solids and Structures*, Vol. 48, No. 16-17, pp. 2349-2360, 2011. DOI: 10.1016/j.ijsolstr.2011.04.012.

[30] Chung, J. and Hulbert, G. M. A time integration algorithm for structural dynamics with improved numerical dissipation: the generalized-α method. *Journal of Applied Mechanics*, Vol. 60, No. 2, pp. 371-375, 1993. DOI: 10.1115/1.2900803.

[31] Jansen, K. E., Whiting, C. H. and Hulbert, G. M. A generalized-α method for integrating the filtered Navier-Stokes equations with a stabilized finite element method. *Computer Methods in Applied Mechanics and Engineering*, Vol. 190, No. 3-4, pp. 305-319, 2000.